

Self-Assembly of Ligated Gold Nanoparticles: Phenomenological Modeling and Computer Simulations[†]

Siddique J. Khan, F. Pierce,[‡] C. M. Sorensen, and A. Chakrabarti*

Department of Physics, Kansas State University, Manhattan, Kansas 66503. [‡] Current address:
Department of Chemistry, Clemson University, 219 Hunter Laboratories, P.O. Box 340973, Clemson,
South Carolina 29634-0973

Received March 6, 2009. Revised Manuscript Received April 16, 2009

We study the assembly of ligated gold nanoparticles by both phenomenological modeling and computer simulations for various ligand chain lengths. First, we develop an effective nanoparticle–nanoparticle pair potential by treating the ligands as flexible polymer chains. Besides van der Waals interactions, we incorporate both the free energy of mixing and elastic contributions from compression of the ligands in our effective pair potentials. The separation of the nanoparticles at the potential minimum compares well with experimental results of gold nanoparticle superlattice constants for various ligand lengths. Next, we use the calculated pair potentials as input to Brownian dynamics simulations for studying the formation of nanoparticle assembly in three dimensions. For dodecanethiol ligated nanoparticles in toluene, our model gives a relatively shallower well depth and the clusters formed after a temperature quench are compact in morphology. Simulation results for the kinetics of cluster growth in this case are compared with phase separations in binary mixtures. For decanethiol ligated nanoparticles, the model well depth is found to be deeper, and simulations show hybrid, fractal-like morphology for the clusters. Cluster morphology in this case shows a compact structure at short length scales and a fractal structure at large length scales. Growth kinetics for this deeper potential depth is compared with the diffusion-limited cluster–cluster aggregation (DLCA) model.

I. Introduction

Colloids of surface-ligated nanoparticles^{1–5} (NP) often act as solutions displaying temperature- and solvent-dependent solubility.^{6,7} A detailed understanding of the interactions between nanoparticles is needed to control the self-assembly of nanoparticles into 2D and 3D superlattices, wetting layers, and films on surfaces and aggregation to a variety of structures including ramified gels and compact superlattice crystals. However, the experimental determination of the forces between ligated nanoparticles still remains a challenging task.

Theoretical modeling of NP–NP interactions can broadly be classified into two groups. In the first group, a coarse-grained approach is taken, and the interaction potential is often written in terms of effective van der Waals interactions between the cores alone.^{8,9} In some work, the free energy of mixing between the tethered chains is also considered.¹⁰ Such a coarse-grained approach to include the free energy of mixing ligands with solvent can be criticized for two reasons. First, the free energy of mixing

typically calculated for polymers end-grafted to flat surfaces and then converted to spherical particles via the Derjaguin approximation. However, the curvature effects of the nanoparticles are quite strong, and the Derjaguin approximation is expected to break down. Moreover, such a calculation typically considers the tethered chains as flexible polymer chains, which might not be a good approximation for the short alkane chains ligated onto nanoparticles.

In the second group of theoretical modeling, a semimacroscopic approach is taken, and NP–NP interactions are calculated directly by numerical simulations.^{11,12} In such simulations, one typically considers two nanoparticles at a fixed distance in the presence of flexible chains that can adsorb onto the nanoparticles with some adsorption energy. The interaction between polymer segments is modeled by the Lennard-Jones potential, and the effective force between two nanoparticles is computed by using a virial relation. A recent study¹² finds that the effect of curvature of the nanoparticles is highly pronounced when the diameter of the nanoparticle (d) is about 5 times the bond length (σ_p) between the adjacent segments in a polymer chain. These types of calculations, however, are also limited by various factors. For example, the modeling of the ligand–ligand and ligand–nanoparticle interactions is phenomenological Lennard-Jones type. In addition, computational time limitations often restrict the choice of the size of the nanoparticles in such simulations. A typical gold nanoparticle has a diameter of about 5 nm whereas the carbon–carbon bond length in an alkane chain is about 0.15 nm. Thus, the ratio of the diameter of the nanoparticle (d) and the bond length (σ_p) between the adjacent segments in a ligand is about 33, which is much larger than the values (typically 5 or 10) used in simulations. In addition, these calculations are extremely

[†] Part of the “Langmuir 25th Year: Nanoparticles synthesis, properties, and assemblies” special issue.

*Corresponding author. E-mail: amitc@phys.ksu.edu.

- (1) Collier, C. P.; Vossmeyer, T.; Heath, J. R. *Annu. Rev. Phys. Chem.* **1998**, *49*, 371.
(2) Aiken, J. D.; Finke, R. G. *J. Mol. Catal., A* **1999**, *145*, 1.
(3) Daniel, M.-C.; Astruc, D. *Chem. Rev.* **2004**, *104*, 293.
(4) Wilcoxon, J. P.; Abrams, B. L. *Chem. Soc. Rev.* **2006**, *35*, 1162.
(5) Prasad, B. L. V.; Sorensen, C. M.; Klabunde, K. J. *Chem. Soc. Rev.* **2008**, *37*, 1871.
(6) Steigerwald, M. L.; Brus, L. E. *Acc. Chem. Res.* **1990**, *23*, 183.
(7) Yan, H.; Cingarapu, S.; Klabunde, K. J.; Chakrabarti, A.; Sorensen, C. M. *Phys. Rev. Lett.* **2009**, *102*, 095501.
(8) Ohara, P. C.; Leff, D. V.; Heath, J. R.; Gelbart, W. M. *Phys. Rev. Lett.* **1995**, *75*, 3466–3469.
(9) Leff, D. V.; Ohara, P. C.; Heath, J. R.; Gelbart, W. M. *J. Phys. Chem.* **1995**, *99*, 7036–7041.
(10) Raghavan, S. R.; Hou, J.; Baker, G. L.; Kahn, S. A. *Langmuir* **2000**, *16*, 1066–1077.

(11) Schapotschnikow, P.; Pool, R.; Vlugt, T. J. H. *Nano Lett.* **2008**, *8*, 2930–2934.

(12) Marla, K. T.; Meredith, J. C. *Langmuir* **2005**, *21*, 487–497.

time-consuming, and often a direct comparison to experimental results is not possible.

Our approach in this article is phenomenological. We treat the ligands as flexible polymer chains and do consider a free energy of mixing approach. In addition, we also consider elastic contributions from compression of the ligands to the effective nanoparticle–nanoparticle pair potential. As discussed earlier, this method has its limitations. However, such a calculation is important for various reasons. First, the separation of the nanoparticles at the potential minimum can be directly compared to experimental results of gold nanoparticle superlattice constants for various ligand lengths. Second, the calculated pair potentials can be used as input to Brownian dynamics simulations to study the formation of nanoparticle assembly. Finally, this type of phenomenological calculation can set a benchmark against which more accurate calculations can be compared.

The rest of the article is organized as follows. In section II, we introduce various components of the interaction potentials that enter into the final effective potential between two nanoparticles. In section III, we evaluate these potentials for various ligand chain lengths and compare the separation of the nanoparticles at the potential minimum to the experimental results of gold nanoparticle superlattice constants. In section IV, we use these pair potentials as input to Brownian dynamics simulations and study the formation of nanoparticle assembly. Clusters obtained in the simulations range from dense, compact morphology to fractal aggregates that show ramified morphology on large scales but hexagonally close-packed crystalline morphology on short length scales. We compare our results of growth kinetics with traditional models of phase separation and diffusion-limited cluster–cluster aggregation (DLCA). Finally, we conclude in section V with a brief summary and discussions of our results.

II. Components of the Effective Nanoparticle–Nanoparticle Interaction Potential

In our phenomenological model, we consider a solution of gold nanoparticles of diameter $d = 5$ nm ligated with various alkane–thiol ligands in toluene. Ligands are considered to be flexible chains, and free energy of mixing and elastic contributions due to ligand compressions are considered in addition to van der Waals interactions.

A. van der Waals Interaction between Two Gold Nanoparticles. The expression for the van der Waals interaction potential between two spherical particles is well known¹³ in the pairwise summing approximation and can be written as

$$V_1 = -\frac{A}{12} \left[\frac{1}{x^2-1} + \frac{1}{x^2} + 2 \ln \left(1 - \frac{1}{x^2} \right) \right] \quad (1)$$

Here, A is the Hamaker constant and x is the rescaled center–center distance between the two particles (i.e., $x = r/d$ where r is the bare center–center distance and d is the diameter of the gold core). In the presence of ligands on the nanoparticles, the effective Hamaker constant between two nanoparticles will have contributions from the bare gold–gold Hamaker constant, the ligand–ligand Hamaker constant (treated as a continuum layer), and the solvent–solvent Hamaker constants. However, the Hamaker constants of the solvent and the ligands are similar to each other and are much smaller than the Hamaker constant for gold. Thus, the effective Hamaker constant between two ligated nanoparticles can be estimated as the gold–gold Hamaker constant through the

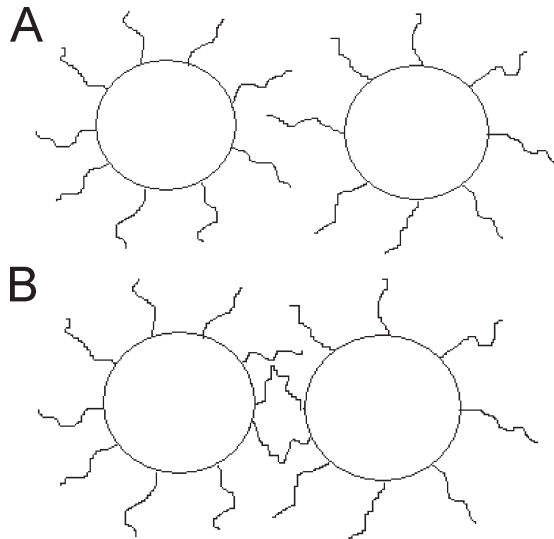


Figure 1. (a) Schematic drawing of the interpenetration of ligand layers from two different nanoparticles. (b) Schematic drawing of the interpenetration and compression of ligand layers from two different nanoparticles.

Table 1. Parameters Used in the Calculations for Dodecanethiol Ligands in Toluene

parameters	value	references
diameter of gold nanoparticle (d)	5 nm	
dodecanethiol ligated Hamaker constant	1.95 eV or $75.5kT$	⁸
contour length of dodecanethiol ligands	$L = 1.774$ nm	¹⁸
size of solvent molecules (toluene)	$v_m = 1.78 \times 10^{-28}$ (m ³)	
Flory χ parameter	$= (V_m/RT)(\delta_s - \delta_m)^2 + \beta_1$; $\beta_1 = 0.34$, where δ_m and δ_s are Hildebrand solubility parameters with values listed in Table 2	¹⁰
surface area of gold covered by a thiol group $A_{\text{thiol,gold}}$	21.5 Å ²	¹⁹

Table 2. Hildebrand Solubility Parameters

solubility parameters	δ values $\times 10^4$ √Pa	references
decane (C ₁₀ H ₂₂)	1.58	¹⁶
dodecane (C ₁₂ H ₂₆)	1.60	¹⁶
hexadecane (C ₁₆ H ₃₄)	1.63	¹⁶
decanethiol (C ₁₀ H ₂₂ S)	1.74	¹⁷
dodecanethiol (C ₁₂ H ₂₆ S)	1.65	¹⁷
hexadecanethiol (C ₁₆ H ₃₄ S)	1.69	¹⁷
toluene	1.82	¹⁶

ligand medium and is taken as $A = 75.5kT$ in our calculations (with $T = 300$ K) as used in a previous study.⁸

B. Free Energy of Mixing. To estimate the free energy of mixing of the ligands when ligand layers from two different nanoparticles start overlapping, one needs to consider two different regimes. In the first regime, the ligand chains undergo interpenetration, and in the second regime, the chains undergo interpenetration and compression. These two regimes are shown schematically in Figure 1a,b, respectively. If the length of the ligands is denoted by L , then these two regimes can be distinguished as

regime I $1 + \tilde{L} < x < 1 + 2\tilde{L}$ (interpenetrations only)

regime II $x < 1 + \tilde{L}$ (interpenetration and compression)

(13) Verwey, E. J. W.; Overbeck, J. T. G. *Theory of Stability of Lyophobic Colloids*; Elsevier: Amsterdam, 1948.

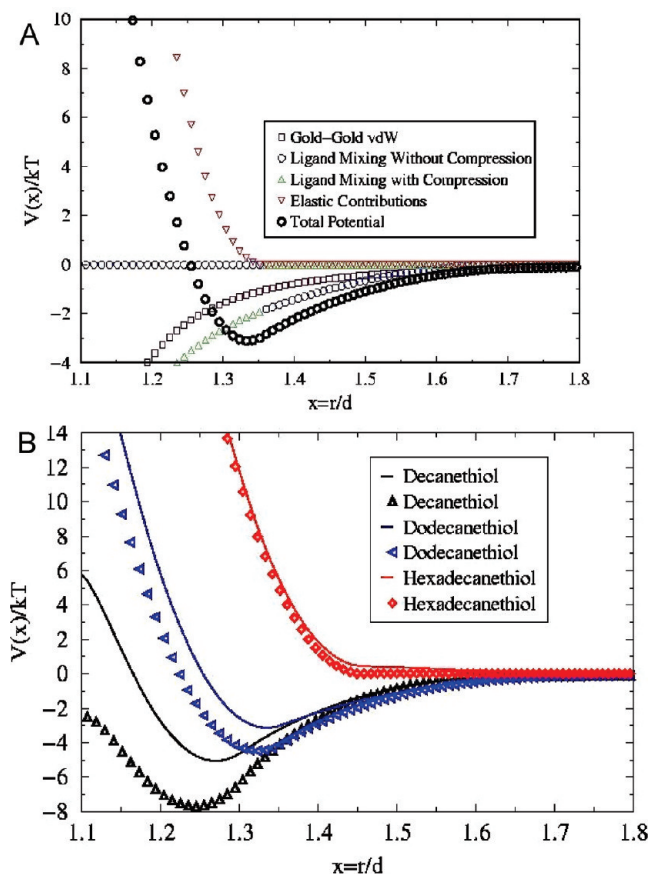


Figure 2. (a) Various components of the interaction potential between two gold nanoparticles with dodecanethiol ligands. (b) Effective interaction potential between two gold nanoparticles with decanethiol, dodecanethiol, and hexadecanethiol ligands. The solid lines are effective potentials with contributions from van der Waals, ligand mixing with and without compression, and elastic compression terms. Symbols are for the effective potentials where the ligand mixing parts of the effective potential have been replaced by the denting potential. (See the text.)

where \tilde{L} is the rescaled length of the ligand chains (i.e., $\tilde{L} = L/d$).

The free energy of mixing in regimes I and II is known in the literature¹⁴ in terms of the Flory χ parameter between the solvent and the tethered chains. In terms of our rescaled variables, one can write this in regime I as

$$\frac{V_2}{kT} = \frac{\pi d^3}{2v_m} \phi_{av}^2 \left(\frac{1}{2} - \chi \right) [x - (1 + 2\tilde{L})]^2; \quad 1 + \tilde{L} < x < 1 + 2\tilde{L} \quad (2)$$

where v_m is the volume of a solvent (toluene) molecule and ϕ_{av} is the average volume fraction of the ligand segments in the tethered layer, which are assumed to have a step profile with a uniform segment density in the layer and a sharp drop to zero segment density outside of the layer.

Similarly in regime II, the free energy of mixing can be written as

$$\frac{V_3}{kT} = \frac{\pi d^3}{v_m} \phi_{av}^2 \left(\frac{1}{2} - \chi \right) \tilde{L}^2 \left[3 \ln \left(\frac{\tilde{L}}{x-1} \right) + 2 \left(\frac{x-1}{\tilde{L}} - \frac{3}{2} \right) \right]; \quad x < 1 + \tilde{L} \quad (3)$$

Note that when $x = 1 + \tilde{L}$, $V_2 = V_3$ as expected.

(14) Smitham, J. B.; Evans, R.; Napper, D. H. *J. Chem. Soc., Faraday Trans. 1* **1975**, *71*, 285–297.

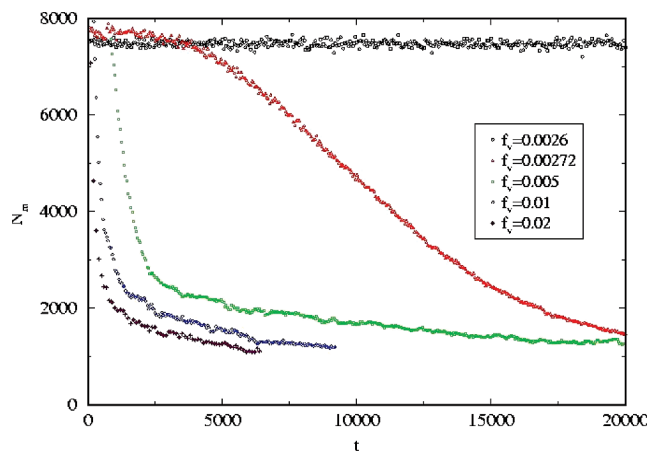


Figure 3. Variation of the number of monomers, left in the system, as a function of time for different volume fractions of gold nanoparticles ligated with dodecanethiol.

C. Elastic Contribution from Ligand Compression. The elastic contribution to the potential due to ligand compression is also known in the literature.¹⁵ On close approach between two nanoparticles, the volume available for the tethered chains to fit is much less than when the two nanoparticles are infinitely separated. This gives rise to a loss of configurational entropy of the tethered chains and leads to an elastic repulsion between two nanoparticles. In terms of the rescaled variables used in this article, this can be written as

$$\frac{V_4}{kT} = \pi v d^2 \left[(x-1) \left(\ln \frac{x-1}{\tilde{L}} - 1 \right) + \tilde{L} \right]; \quad x < 1 + \tilde{L} \quad (4)$$

where v is the number of ligands per unit area of the nanoparticle.

III. Evaluation of the Effective NP–NP Interaction Potential

We compute the effective pair potential between two nanoparticles in toluene with decanethiol, dodecanethiol, and hexadecanethiol ligands, respectively. The parameters used in the calculations for dodecanethiol in toluene are listed^{16,17} in Tables 1 and 2. The parameters for the other two cases are similar.¹⁸ The value of v , the number of ligands per unit area of the nanoparticle, is calculated from the estimated surface area of gold covered by a thiol group,¹⁹ $A_{thiol,gold}$, as $v = 1/(21.5(10^{-10} \text{ m})^2) = 4.65 \times 10^{18} \text{ m}^{-2}$, and the number of ligands per nanoparticle is $N \approx A_{surface,gold}/A_{thiol,gold} \approx 365$. Assuming that dodecanethiol has a molecular volume found from its molar weight and density of $\sim 3.98 \times 10^{-28} \text{ m}^3$, we can find an estimate for ϕ_{av} . The ligand shell extends from $r = d/2$ ($= 2.5 \text{ nm}$) up to $r = d_0/2 + L$ ($\sim 4.3 \text{ nm}$). This shell has a volume of $V_{shell} \approx 2.68 \times 10^{-25} \text{ m}^3$. Then $NV_{dodecane}/V_{shell} \approx 365 (3.98 \times 10^{-28})/(2.68 \times 10^{-25}) \approx 0.54$.

In the model calculation, we have assumed that the contributions to the free energy of mixing for ligand–ligand interpenetration originates only from the alkane-chain part of the ligands whereas the thiol group is firmly attached to the gold

(15) Evans, R.; Smitham, J. B.; Napper, D. H. *Colloid Polym. Sci.* **1977**, *255*, 161–167.

(16) Brandrup, J.; Immergut, E. H.; Gruike, E. A. *Polymer Handbook*; Wiley: New York, 1999.

(17) Yaws, C. L. *Chemical Properties Handbook*; McGraw Hill: New York, 1999.

(18) (a) Motte, L.; Billouet, F.; Pileni, M. P. *J. Phys. Chem.* **1995**, *99*, 16425–16429. (b) Bain, C. D.; Evall, J.; Whitesides, G. M. *J. Am. Chem. Soc.* **1989**, *111*, 7155.

(19) Poirier, G. E.; Pylant, E. D. *Science* **1996**, *272*, 1145–1148.

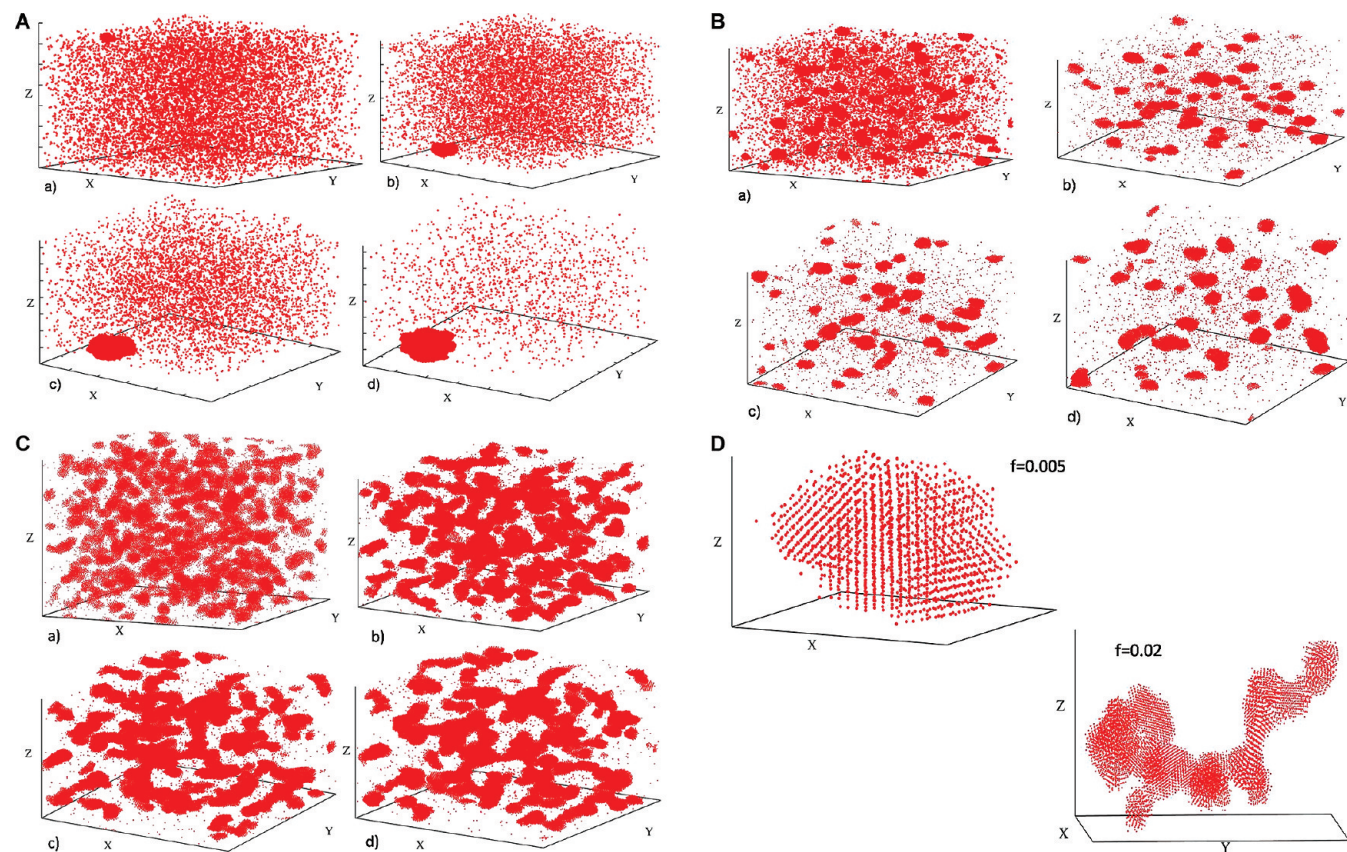


Figure 4. (A) Simulation snapshots for dodecanethiol-ligated nanoparticles at different times for a critical volume fraction of $f_c = 0.00272$: (a) $t = 3000$, (b) $t = 5000$, (c) $t = 10000$, and (d) $t = 20000$. (B) Simulation snapshots for dodecanethiol-ligated nanoparticles at different times for a volume fraction of $f = 0.005$: (a) $t = 1000$, (b) $t = 3000$, (c) $t = 5000$, (d) $t = 10000$. (C) Simulation snapshots for dodecanethiol-ligated nanoparticles at different times for a volume fraction of $f = 0.02$: (a) $t = 500$, (b) $t = 1000$, (c) $t = 4500$, (d) $t = 6000$. (D) Close-up structures of dodecanethiol ligated nanoparticle clusters for volume fractions of $f = 0.005$ and 0.02 .

surface and does not play any role in this interaction. This is why we have used the solubility parameter values of unthiolated alkane chains (i.e., for $C_{10}H_{22}$) instead of those for thiolated chains ($C_{10}H_{22}S$) in Table 2. If we instead use the solubility parameters for the thiolated chains, the effective NP–NP potentials become too shallow and the NPs would not assemble as superlattices.

In addition to ligand interpenetration and compression, we have also considered a possible situation in which ligand layers are compressed without any interpenetration only when two nanoparticles are in close contact. This layer conformation is known as “denting” in the literature.¹⁴ In Figure 2b, we have shown our phenomenological model in comparison with the denting potential, according to which when particles collide their ligand layers are compressed. In the denting model, the ligand free energy of mixing potentials V_2 and V_3 is replaced by a denting potential given by

$$\frac{V_{\text{denting}}}{kT} = 4 \frac{\pi d^3}{v_m} \phi_{\text{av}}^2 \left(\frac{1}{2} - \chi \right) \tilde{L}^2 \left[\ln \left(\frac{2\tilde{L}}{x-1} \right) + \left(\frac{x-1}{2\tilde{L}} \right) - 1 \right]; 1 < x < 1 + 2\tilde{L} \quad (5)$$

The symbols in Figure 2b show the effective potential curves for the denting potential whereas the solid lines show the respective curves for our phenomenological model. One observes that the potential wells are deeper for the denting potential for all of the ligand lengths considered in this study. The variation in the potential depth for hexadecanethiol and dodecanethiol

ligands are not substantial. However, for the decanethiol ligands, the potential well becomes totally negative without any energy barrier to the primary van der Waals minimum. This is not a realistic description of the NP–NP interaction because decanethiol ligated gold nanoparticles do form superlattices.²⁰ We thus conclude that the denting potential is not a good alternative to the phenomenological model considered in this article.

In Figure 2a, we show various contributions to the effective potential for the dodecanethiol ligands. The location of the minimum of the potential compares extremely well to the superlattice constant calculated in experiments. In Figure 2b, we show the effective potential for three different ligand lengths. For dodecanethiol and hexadecanethiol, the location of the minimum of the effective pair potential agrees well with the superlattice constant seen in experiments. In addition, it is known experimentally that the solubility of gold NP in toluene improves with increasing ligand length. This is consistent with the trend seen in Figure 2b because the depth of the potential becomes shallower as the ligand length is increased.

IV. Brownian Dynamics Simulation with an Effective Nanoparticle–Nanoparticle Interaction Potential

A. Simulation Method. We have carried out Brownian dynamics (BD) simulations²¹ in three dimensions (3D) to

(20) Prasad, B. L. V.; Stoeva, S. I.; Sorensen, C. M.; Klabunde, K. J. *Langmuir* 2002, 18, 7515–7520.

(21) Van Gunsteren, W. F.; Berendsen, H. J. C. *Mol. Phys.* 1982, 45, 637.

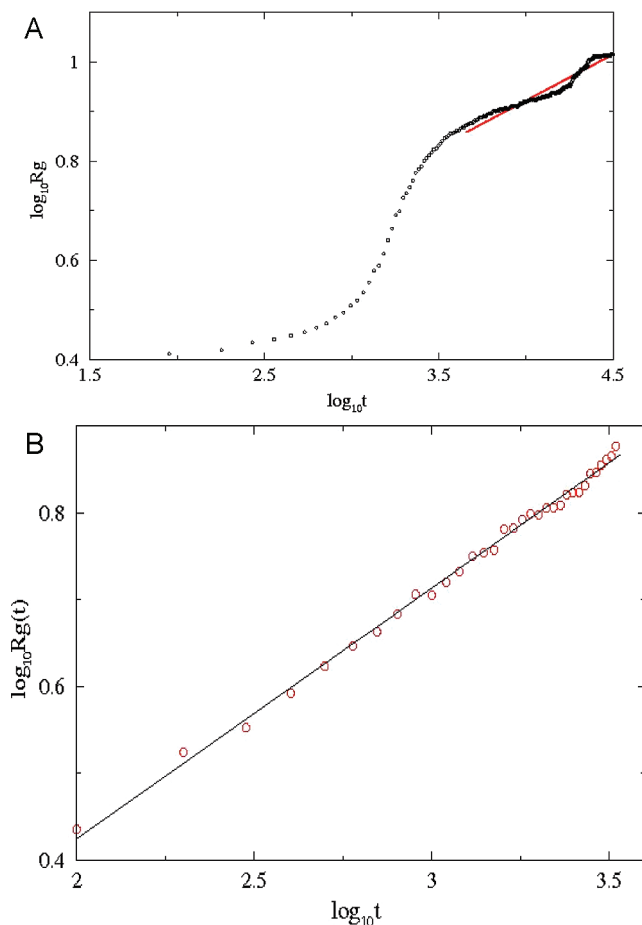


Figure 5. (a) Log–log plot of the radius of gyration (R_g) versus time for dodecanethiol-ligated nanoparticles. Here the volume fraction is $f = 0.005$. The solid line yields an exponent of ~ 0.16 . Even after averaging over 10 runs, the statistics are poor here because there are relatively few clusters formed at this volume fraction. Simulations with a much larger system would be necessary to get better statistics on the clusters at long times. (b) Log–log plot of the radius of gyration (R_g) versus time for dodecanethiol-ligated nanoparticles. Here the volume fraction is $f = 0.02$. The solid line yields an exponent of ~ 0.3 .

study the assembly of dodecanethiol ligated gold nanoparticles. The equations of motion for the BD simulation read as

$$\ddot{\vec{r}}_i = -\vec{\nabla} U_i - \Gamma \dot{\vec{r}}_i + \vec{W}_i(t)$$

where Γ is the friction coefficient and W_i , the random force acting on each colloidal particle i , is Gaussian white noise satisfying a fluctuation–dissipation relation. The potential U is modeled as an effective pair-potential shown in Figure 2b (i.e., a mixture of van der Waals, ligand mixing, and elastic terms as discussed earlier in the article). The potential is set to zero for $x \geq 1.8$.

We set particle diameter $d = 1$ and measure all distances in units of d . We choose $\Gamma = 0.5$ and time step $\Delta t = 0.005$ in reduced time units of $d(m/kT)^{1/2}$ with $m = 1$. Periodic boundary conditions are enforced to minimize wall effects. Several different values of monomer concentrations over a range of $f = 0.0001$ to 0.02 are used in the simulations with the number of nanoparticles used being up to 80 660 in some runs. All simulations start from a random initial monomer conformation, and the results for the kinetics are averaged over 5–10 runs.

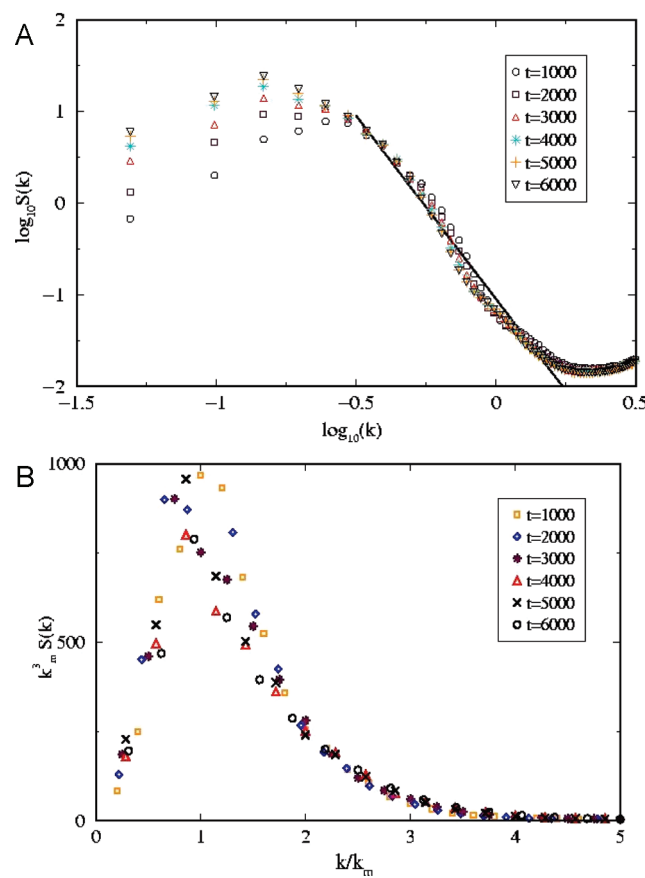


Figure 6. (a) Log–log plot of the structure factor at different times for dodecanethiol-ligated nanoparticles. Here the volume fraction is $f = 0.02$. The solid line yields a slope of -4 (Porod’s law), indicating the compact structure of the clusters at both short and large length scales. Deviations from Porod’s law might arise from finite-size effects. Simulations of a much larger system size would be necessary to get more accurate results for the structure factor. (b) Dynamical scaling plot for the structure factor (see text) for dodecanethiol-ligated nanoparticles. Here the volume fraction is $f = 0.02$.

Hydrodynamic interactions, including lubrication forces, are ignored in the simulation because they might not be of predominant importance for a study of quiescent secondary minimum colloids.²²

B. Nanoparticle Assembly with Dodecanethiol Ligands. *1. Estimation of Critical Volume Fraction for Nucleation.* Transition from a dispersed phase to a state in which the solid phase starts to develop is observed in the simulations when the monomer volume fraction f is larger than a critical value f_c . For computing cluster properties, we consider two neighboring particles to belong to the same cluster if the distance between their centers is less than or equal to the range of the interaction. In Figure 3, we show the number of monomers left in the system as a function of time after the initial quench for various values of monomer volume fraction f . Because the temperature of the quench is the same for all of these volume fractions, we expect that the final number of monomers left would be the same in the two-phase region. For $f < 0.0027$, the number of monomers left remains fairly constant, indicating the absence of cluster formation within the simulation time. After an initial waiting period, the growth of only one round-shaped cluster amidst a gas phase is observed in Figure 4a for $f = 0.0027$.

(22) (a) Nguyen, N. Q.; Ladd, A. J. C. *Phys. Rev. E* **2002**, 66, 046708. (b) Brady, J. F. *J. Chem. Phys.* **1993**, 99, 567. (c) Reese, D. O.; et al. *Phys. Rev. Lett.* **2000**, 85, 5460.

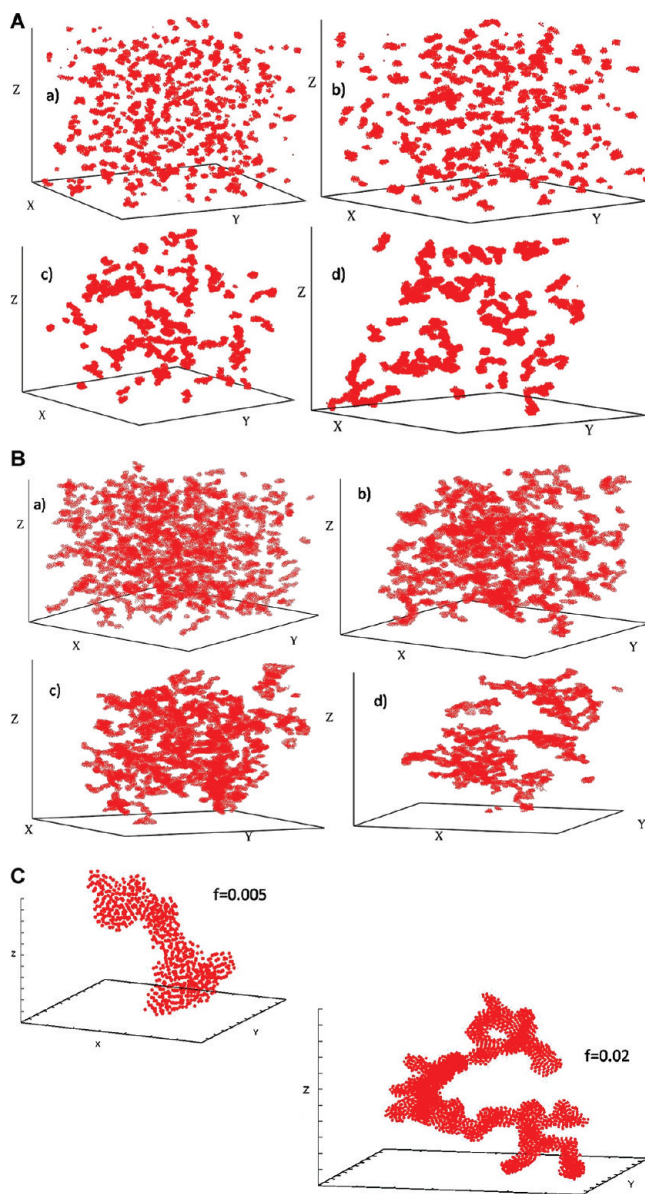


Figure 7. (A) Simulation snapshots for decanethiol-ligated nanoparticles at different times for a volume fraction of $f = 0.005$: (a) $t = 500$, (b) $t = 1000$, (c) $t = 5000$, (d) $t = 10000$. (B) Simulation snapshots for decanethiol-ligated nanoparticles at different times for a volume fraction of $f = 0.02$: (a) $t = 500$, (b) $t = 2000$, (c) $t = 3000$, (d) $t = 4000$. (C) Close-up structure of decanethiol-ligated nanoparticle clusters for volume fractions of $f = 0.005$ and 0.02 .

For $f > 0.0027$, several clusters nucleate and grow with time. This can be seen in Figure 4b for $f = 0.005$, for example. For a dense system (such as shown in Figure 4c for $f = 0.02$), the morphology of domains is quite similar to the interconnected structure seen in a typical spinodal decomposition of a liquid–liquid mixture. In Figure 4d, we show the details of the close-packing structure of the clusters by focusing on one individual cluster for both $f = 0.005$ and 0.02 .

We have carried out several runs for different volume fractions ranging from 0.002 to 0.03 where we have considered only the van der Waals interaction potential (V_1) and the elastic contribution from ligand compression (V_4), neglecting contributions from the free energy of mixing of the ligands. We have not observed any cluster formation even in the highest volume fraction case. Although direct experimental studies of high

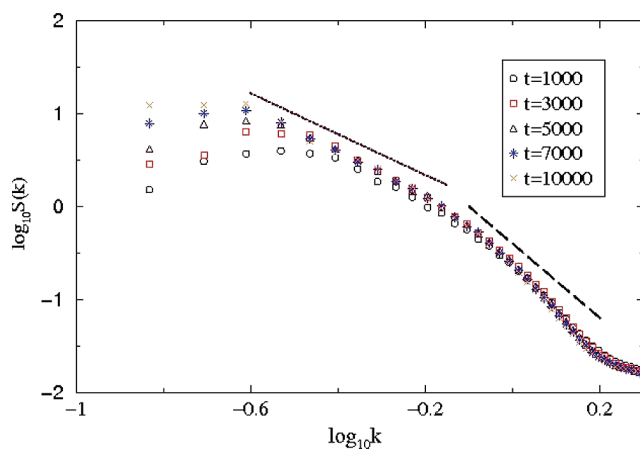


Figure 8. $\log-\log$ plot of the structure factor at several times for decanethiol-ligated nanoparticles with $f = 0.005$. The two dashed lines yield exponents of ~ -1.8 and ~ -4 , respectively, indicating the hybrid nature of the clusters with a short length scale compact structure and a large length scale DLCA-type fractal structure.

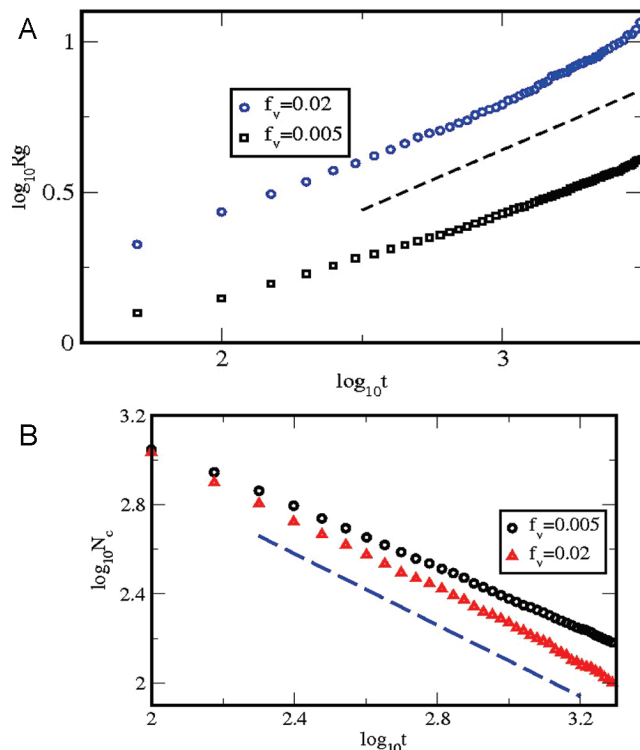


Figure 9. (a) $\log-\log$ plot of the radius of gyration (R_g) versus time for decanethiol-ligated nanoparticles with $f = 0.005$ and 0.02 . The dotted line yields an exponent of ~ 0.45 . (b) $\log-\log$ plot of the number of clusters (N_c) versus time for decanethiol-ligated nanoparticles with $f = 0.005$ and 0.02 . The dotted line yields an exponent of ~ -0.8 .

monomer concentration in solution are not found in the literature, superlattices do form in nanoparticle solutions (on a TEM grid for example) where the solvent is allowed to evaporate, resulting in a dense system. We can thus reasonably conclude that just the van der Waals interaction among nanoparticles is not sufficient to describe NP–NP interactions in the model system considered here and that the free energy of mixing term for the ligands plays an important role, particularly in dense systems.

2. Growth Kinetics. In Figure 5a,b, we show $\log-\log$ plots of the average radius of gyration R_g of the clusters as a function of time for $f = 0.005$ and 0.02 , respectively. For $f = 0.005$, we see

three regimes in the growth kinetics. First, there is an induction period ($t \leq 300$) where droplets of critical size are yet to nucleate. This is followed by sudden fast growth corresponding to the heterogeneous nucleation of many clusters ($300 \leq t \leq 3000$). Subsequently, these clusters grow with time with a power law of $R_g \approx t^n$ with $n \approx 0.16$. Although the data at this stage show large fluctuations even after averaging over 10 runs, one can understand the observed value of the exponent n in the following way. As first suggested by Binder and Stauffer²³ and nicely summarized by Furukawa,²⁴ the domain growth kinetics at this stage is mostly controlled by surface reorganization of the clusters in order to reduce interfacial tension. In such a case of domain growth, one obtains $n = 1/(D + 3)$ where $D = 3$ is the spatial dimension of the system. Our observed value of $n \approx 0.16$ agrees with the theoretical prediction.

In contrast, for $f = 0.02$, $R_g \approx t^n$ with $n \approx 0.3$ over a long period of time. This value of the exponent is consistent with a domain growth exponent of $n = 1/3$ in the spinodal decomposition of off-critical liquid–liquid mixtures²⁵ (when hydrodynamic interactions are not important). In Figure 6a, we show the log plot of the structure factor $S(k, t)$ versus k . A fit to the data shows that $S(k)$ is consistent with Porod's law ($S(k) \approx k^{-4}$) over a large range of k values, confirming our direct observations that the growing clusters are compact at both short and large length scales.

Phase-separation processes in liquid mixtures can be described by a dynamical scaling form with a time-dependent characteristic length.²⁵ A major feature of this description is that the structure factor $S(k, t)$ can be written in a time-independent dynamical scaling form

$$k_m^d(t)S(k, t) = F[k/k_m(t)]$$

where $k_m(t)$ is the location of the peak in the structure factor and is a measure of the (inverse) characteristic length in the system. We have tested the dynamical scaling hypothesis for domain growth in quenched nanoparticle solutions for $f = 0.02$. The results are shown in Figure 6b. Reasonably good scaling is observed in the simulation over the time interval shown in the Figure. We also note that the quality of scaling actually improves at late times.

C. Nanoparticle Assembly with Decanethiol Ligands. In this case, the potential well depth is deeper than for the previous case studied in our simulations. For both $f = 0.005$ and 0.02, the large-scale morphology is fractal-like as seen in Figure 7a,b whereas the short-range close-packed ordering becomes clear as we focus on individual clusters (Figure 7c). Such hybrid morphology of clusters has previously been seen in both simulations^{26,27} and experiments^{28,29} of colloidal self-assembly.

The hybrid morphology of the clusters observed in real space leaves its mark on the structure factor as well. In Figure 8, we show the log plot of structure factor $S(k, t)$ versus k . A fit to the data shows that $S(k)$ is consistent with Porod's law ($S(k) \approx k^{-4}$) for large k values, whereas for intermediate values of k , $S(k) \approx k^{-D_f}$ with $D_f \approx 1.8$ consisting of the well-known diffusion-limited cluster–cluster aggregation (DLCA) value.³⁰ This confirms our

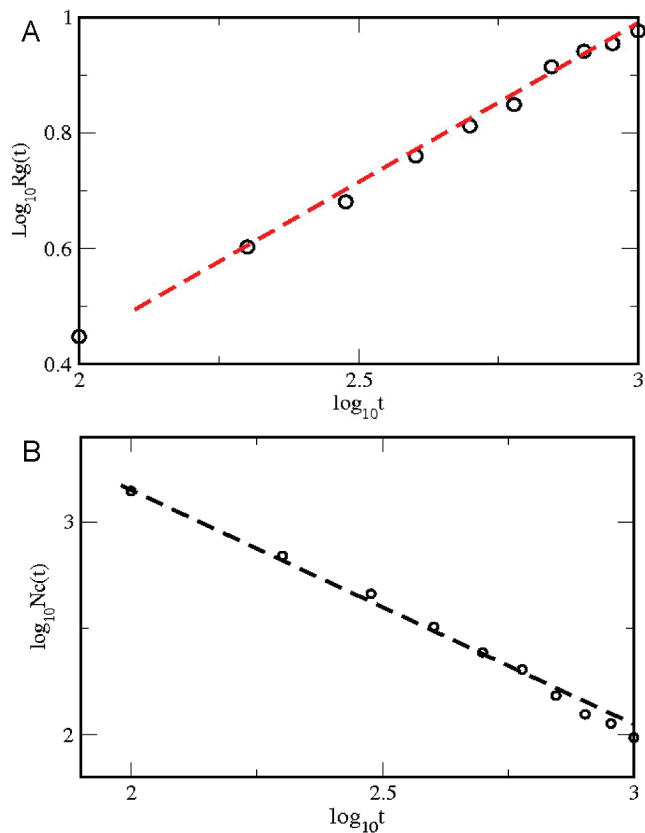


Figure 10. (a) log–log plot of the radius of gyration (R_g) versus time for deeply quenched decanethiol-ligated nanoparticles with $f = 0.02$. The solid line yields an exponent of ~ 0.55 . (b) log–log plot of the number of clusters (N_c) versus time for deeply quenched decanethiol-ligated nanoparticles with $f = 0.02$. The dotted line yields an exponent of ~ -1 .

direct observations that the growing clusters are compact at short length scales but are fractal-like at large length scales.

For fractal cluster growth in the traditional DLCA model, one can use kinetic theory based on the Smoluchowski equation for irreversible aggregation.³¹ At late times, one finds that the mean cluster size grows as $s(t) \approx t^z$ where the kinetic exponent is $z = 1$ for Brownian coagulation. Because the total number of monomers is fixed in the system, the number of clusters N_c then decays with time as $N_c \approx t^{-z}$. In addition, if the fractal dimension of the clusters is given by D_f , then $s \approx R_g^{D_f}$ or $R_g \approx t^n \approx t^{z/D_f}$ with time, yielding $n = z/D_f$. For the 3D DLCA model, $D_f \approx 1.8$ and one finds $n \approx 0.55$.

Our results for R_g versus t and N_c versus t are shown in Figure 9a,b in the log–log plots. Figure 9a shows the temporal evolution of R_g for volume fractions of 0.005 and 0.02. Both curves yield a slope of 0.45. In Figure 9b, the variation of the number of clusters N_c with time is plotted on a log–log scale. The curves yield a slope of -0.8 . From the kinetic exponents observed in Figure 9a,b, it seems that although the potential well is deeper for the decanethiol ligand case the growth kinetics still does not belong to the pure DLCA model.

To test whether the DLCA model is truly recovered when the potential well depth is extremely deep, we set $kT = 0.5kT_{\text{room}}$ in the next set of simulations. This would make the minimum of the potential well depth equivalent to $\approx 10kT_{\text{room}}$. Results for such a

(23) Binder, K.; Stauffer, D. *Phys. Rev. Lett.* **1974**, 33, 1006.

(24) Furukawa, H. *Adv. Phys.* **1985**, 34, 703–750.

(25) (a) Gunton, J. D. In *Phase Transitions and Critical Phenomena*; Domb, C., Lebowitz, J. L., Eds.; Academic Press: London, 1983; Vol. 8. (b) Bray, A. J. *Adv. Phys.* **1994**, 43, 357.

(26) Chakrabarti, A.; Fry, D.; Sorensen, C. M. *Phys. Rev. E* **2004**, 69, 031408.

(27) Cerda, J. J.; Sintes, T.; Sorensen, C. M.; Chakrabarti, A. *Phys. Rev. E* **2004**, 70, 011405.

(28) Skjeltorp, A. T. *Phys. Rev. Lett.* **1987**, 58, 1444.

(29) Zuckerman, E. B.; Olivier, B. J.; Sorensen, C. M.; Klabunde, K. J. *Chem. Mater.* **1989**, 1, 12.

(30) For a review, see, for example, Meakin, P. *J. Sol-Gel Sci. Technol.* **1999**, 15, 97.

(31) Friedlander, S. K. *Smoke, Dust, and Haze: Fundamentals of Aerosol Dynamics*; Oxford University Press: New York, 2000.

deep quench are shown in Figure 10a,b. It is exciting to observe that indeed, irreversible DLCA model results are recovered in the limit of deep potential well depths.

V. Summary and Conclusions

We have developed a phenomenological model to describe the interactions between two ligated nanoparticles in solution. Besides the van der Walls interaction between the nanoparticles, we also consider the free energy of mixing and elastic compression of the ligands in the model. The location of the minimum of the phenomenological pair potential agrees well with the experimentally observed values for the superlattice constants for gold nanoparticles decorated with decanethiol, dodecanethiol, and hexadecanethiol ligands.

Next we use the model potential as input for Brownian dynamics simulations to obtain a broad perspective in the dispersed-phase to solid-phase transition. For dodecanethiol-ligated nanoparticles, the minimum of the interaction potential is $\sim -3.1kT$. At constant temperature, the system remains in the single phase until a critical volume fraction is reached, when the nucleation of round clusters starts. At higher volume fractions, round clusters are found to coexist with the dispersed

phase. The kinetics of cluster growth in this case is compared with phase separations in binary mixtures.

For decanethiol-ligated nanoparticles, the model well depth is found to be deeper ($\sim -5.15kT$), and simulations show hybrid, fractal-like morphology for the clusters. Cluster morphology in this case shows a compact structure at short length scales and a fractal structure at large length scales. The growth kinetics for this deeper potential depth is compared with the diffusion-limited cluster-cluster aggregation (DLCA) model.

There is very little experimental work available in the literature on the kinetics of self-assembly of nanoparticles. This is why a comparison of our Brownian dynamics simulation results to experiments is not possible at this time. However, very recently two papers^{32,33} have been published on the nucleation of nanoparticle clusters. Our model is quite suitable to study the nucleation of gold nanoparticle clusters, and we are planning to address this issue in our future work.

Acknowledgment. This work was supported by NSF NIRT grant CTS0609318. We thank Professors C. Aakeroy, K. Klabunde, and B. M. Law for many useful discussions.

(32) Abécassis, B.; Testard, F.; Spalla, O. *Phys. Rev. Lett.* **2008**, *100*, 115504.

(33) Yan, H.; Cingarapu, C.; Klabunde, K.; Chakrabarti, A.; Sorensen, C. M. *Phys. Rev. Lett.* **2009**, *102*, 095501.